# Reply to Comment by Y. Kovalyshen on "Ultrasonic Monitoring of Spontaneous Imbibition Experiments: Precursory Moisture Diffusion Effects Ahead of Water Front"

Christian David, Christophe Barnes, Joël Sarout, Jérémie Dautriat, Lucas Pimienta

Journal of Geophysical Research: Solid Earth

REPLY

10.1029/2018JB016133

**Special Section:**
Seismic and Micro-Seismic Signature of Fluids in Rocks: Bridging the Scale Gap

This article is a reply to a comment by Kovalyshen (2018) https://doi.org/10.1029/2018JB016040.

**Key Points:**

- The wave interaction explanation suggested by Kovalyshen (2018) was tested on the complete data set of David et al. (2017)
- We calculated the coefficients of reflection for the *P* wave reflected on the water front and show that they have a small magnitude
- Simulations of composite waveforms show that only 25% of the tested samples might have been impacted by the proposed mechanism

**Correspondence to:**
C. David,
christian.david@u-cergy.fr

**Citation:**
David, C., Barnes, C., Sarout, J., Dautriat, J., & Pimienta, L. (2018). Reply to Comment by Y. Kovalyshen on "ultrasonic monitoring of spontaneous imbibition experiments: Precursory moisture diffusion effects ahead of water front". *Journal of Geophysical Research: Solid Earth*, *123*. https://doi.org/10.1029/2018JB016133

Received 22 MAY 2018
Accepted 7 JUN 2018
Accepted article online 27 JUL 2018



# Reply to Comment by Y. Kovalyshen on "Ultrasonic Monitoring of Spontaneous Imbibition Experiments: Precursory Moisture Diffusion Effects Ahead of Water Front"

**Christian David[1], Christophe Barnes[1], Joël Sarout[2], Jérémie Dautriat[2], and Lucas Pimienta[3]**

[1]Laboratoire Géosciences et Environnement Cergy, Université de Cergy-Pontoise, Cergy-Pontoise, France, [2]CSIRO Energy, Perth, Australia, [3]Laboratory of Experimental Rock Mechanics (LEMR), ENAC, EPFL, Lausanne, Switzerland

**Abstract** We tested on a data set including 12 different rocks the assumption that, during water imbibition experiments, the interaction between direct *P* waves and reflected *P* waves on the imbibition front could explain the early *P* wave amplitude variation occurring before any velocity variation. Our calculations show that (i) the observed distance between the water front and the ultrasonic sensors is always larger than the estimated critical distance below which the first peak amplitude is impacted by the reflected *P* wave, (ii) the magnitude of the coefficients of reflection is generally very small, and (iii) using simulations of composite waveforms, an impact on the first peak amplitude is expected only in 25% of the tested samples. *P* wave interaction is definitively a mechanism which can lead to amplitude variations, but it is very likely that such a mechanism is not responsible for the early amplitude variation detected in most of the tested rocks. Moisture diffusion is still a very relevant mechanism to account for our observations on *P* wave amplitude variations during capillary rise.

## 1. Introduction

In our recent paper (David, Sarout, et al., 2017) results from series of spontaneous imbibition experiments on 14 different rocks with simultaneous ultrasonic monitoring using two pairs of ultrasonic *P* wave sensors were presented. The analysis of the evolution of *P* waves attributes during the imbibition showed in particular that the *P* wave amplitude is systematically impacted before velocity is and that this early amplitude drop occurs when liquid water appears to be located well below the *P* wave transducers. This precursory amplitude variation was explained by the effect of moisture diffusion ahead of the front of liquid water, which seemed to account well for the experimental observations. Assuming that the early amplitude drop is associated with water vapor diffusion in the pore space, the effective diffusivity of moisture in rocks could be estimated, and it was shown that the effective moisture diffusivity derived from ultrasonic data correlates well with permeability in a range spanning 2 orders of magnitude. In a comment on this paper, Kovalyshen (2018) proposes an alternative explanation based on a plane wave assumption (ray theory), source and receiver considered as points, and a perfect planar interface between the dry and wet media. This explanation considers the interaction between the direct *P* wave and the reflected *P* wave on the imbibition front, which could explain the observed amplitude drop while the velocity would not be affected. According to his analysis, such interaction would impact the amplitude of the first recorded peak when the distance between the transducers and the imbibition front is smaller than a critical distance $z_c$ such as $z_c = 0.5\sqrt{(\lambda L)/2}$, where $L$ is the spacing between the *P* wave sensors and $\lambda$ is the wavelength. The author presented an illustration of the potential wave interference using, to our knowledge, a synthetic waveform and assumptions on the rock properties for estimating the reflection coefficient. The purpose of this reply is to test the explanation proposed by Kovalyshen (2018) on our complete data set, in order to assess (or not) its validity, keeping the same assumptions framework.

## 2. Methodology

### 2.1. Estimation of the Critical Distance

The experiments reported in our recent papers (David et al., 2017; David, Sarout, et al., 2017) combined imaging and ultrasonic monitoring; therefore, we are able to link each recorded waveform to the position of the

**Table 1**
*Parameters Used to Estimate the Critical Distance $z_c$ and the Coefficient of Reflection $R_{PP}$ for All the Samples*

| Sample | Porosity (%) | Sensors spacing $L$ (mm) | Wavelength $\lambda$ (mm) | Dry density (kg/m$^3$) | $P$ wave velocity of dry rock (m/s) | $S$ wave velocity of dry rock (m/s) | Dry $V_P/V_S$ ratio | Wet density for $S_w$ = 70% (kg/m$^3$) | $P$ wave velocity of wet rock (m/s) | $S$ wave velocity of wet rock (m/s) |
|---|---|---|---|---|---|---|---|---|---|---|
| SMX | 37.0 | 39 | 5.48 | 1,693 | 2,740 | 1,827 | 1.50 | 1,952 | 2,603 | 1,701 |
| CSG | 25.1 | 26.3 | 3.32 | 1,950 | 1,660 | 1,180 | 1.41 | 2,125 | 1,328 | 1,130 |
| MAJ | 30.0 | 39 | 4.20 | 1,897 | 2,100 | 1,300 | 1.62 | 2,107 | 1,932 | 1,234 |
| SH-ver | 30.0 | 39 | 3.60 | 1,800 | 1,800 | 1,000 | 1.80 | 2,010 | 1,530 | 946 |
| LEO | 21.1 | 26.2 | 5.14 | 2,014 | 2,570 | 1,850 | 1.39 | 2,162 | 2,390 | 1,786 |
| SH-hor | 30.0 | 39 | 2.80 | 1,800 | 1,400 | 810 | 1.73 | 2,010 | 1,260 | 767 |
| SID | 14.3 | 26.6 | 10.48 | 2,336 | 5,240 | 2,940 | 1.78 | 2,436 | 6,078 | 2,879 |
| BER | 18.6 | 27.4 | 4.48 | 2,096 | 2,240 | 1,670 | 1.34 | 2,227 | 2,016 | 1,620 |
| CAT | 16.6 | 27.9 | 4.32 | 2,202 | 2,160 | 1,510 | 1.43 | 2,318 | 2,484 | 1,472 |
| EDB | 25.9 | 27.3 | 7.12 | 2,024 | 3,560 | 2,300 | 1.55 | 2,205 | 3,489 | 2,203 |
| SAV | 32.2 | 26.6 | 6.32 | 1,845 | 3,160 | 1,870 | 1.69 | 2,071 | 3,034 | 1,765 |
| TUF | 38.9 | 26.7 | 3.84 | 1,551 | 1,920 | 1,680 | 1.14 | 1,824 | 1,536 | 1,550 |

*Notes*. The samples are those studied by David, Sarout, et al. (2017).

imbibition front in the sample. In particular the distance $d_A$ between the planes where the transducers are located (planes 1 and 2; see Figure 2a in David, Sarout, et al., 2017) and the position of the imbibition front were measured and reported in Table 2 in David, Sarout, et al. (2017). This measured distance can be compared to the critical distance as defined by Kovalyshen (2018). Note that the critical distance given by Kovalyshen (2018) in his equation (1) is an approximation valid only when the distance to the front is small compared to the sensors spacing $L$. Here we use the full calculation of the critical distance $z_c$ without any approximation:

$$z_c = 0.5\sqrt{\left(\frac{\lambda}{4}+L\right)^2 - L^2} \tag{1}$$

The wavelength $\lambda$ is obtained from the $P$ wave velocity of the dry samples and the resonance frequency of the ultrasonic transducers (0.5 MHz). Following Kovalyshen (2018), an impact of the reflected $P$ wave is expected when the condition $d_A < z_c$ is met. The parameters needed to calculate the critical distance are given in Table 1.

### 2.2. Interaction Between Direct and Reflected *P* Waves

As we recorded the $P$ wave waveform $W(t)$ of the dry sample before the beginning of imbibition, we can build a composite waveform $W_i(t)$ accounting for the interaction between direct and reflected $P$ waves by adding to $W(t)$ a synthetic waveform representing the reflected $P$ wave on the imbibition front:

$$W_i(t) = W(t) + R_{\mathrm{pp}} \times W(t - t_R) \tag{2}$$

where $t_R$ is the time delay between reflected and direct $P$ waves in the dry rock at the time when the amplitude variation was detected:

$$t_R = \left(\sqrt{L^2 + 4d_A^2} - L\right)/V_P^{(\mathrm{dry})} \tag{3}$$

and $R_{\mathrm{PP}}$ is the coefficient of reflection. To calculate the coefficient of reflection, the complete solution for the amplitude of reflected and transmitted $P$ and $S$ waves derived from the Knott-Zoeppritz equations (e.g., given by Mavko et al., 2009) was used. For that purpose, one needs to know (i) the $P$ and $S$ wave velocities and the density of both the dry and the water-wet samples and (ii) the angles of the incident, reflected and transmitted waves. Note that in the Knott-Zoeppritz approach, the propagating waves are assumed to be plane waves. $P$ and $S$ wave velocities and density were measured on the dry samples. For the wet samples after imbibition (which are not fully water-saturated) the density

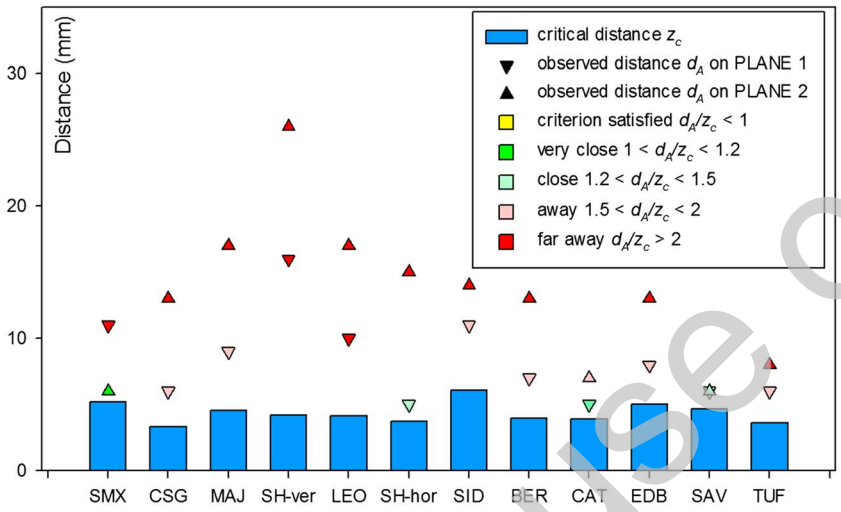


**Figure 1.** Distance of the water front to the transducers plane (triangles) compared to the critical distance (blue bars). The upward triangles are for plane 2; the downward triangles are for plane 1.

$\rho^{(\mathrm{wet})}$ was not measured: We estimate it from the dry density $\rho^{(\mathrm{dry})}$ as $\rho^{(wet)} = \rho^{(dry)} + \phi S_w \rho^{(water)}$ with $\phi$ the porosity, $\rho^{(\mathrm{water})}$ the density of water, and $S_w$ the water saturation, assuming a constant value of 70% for all the samples (comparable to the measured values on a set of sandstones and carbonate rocks in David et al., 2013). Indeed imbibition processes lead to partial saturation because of air trapping in pores (David et al., 2011). The $P$ wave velocity of the wet samples was measured, but not the $S$ wave velocity: We estimate it, assuming that the shear modulus remains constant, leading to $V_S^{(wet)} = V_S^{(dry)} . \sqrt{\rho^{(dry)}/\rho^{(wet)}}$. The parameters needed to compute the coefficient of reflection $R_{\mathrm{PP}}$ are given in Table 1. Note that the $V_P/V_S$ ratios measured in the dry sample are very different from the one used by Kovalyshen (2018) in his simulation ($V_P/V_S = 2$).

The angle of the incident wave is known from the geometry; the other angles are given by Snell's law. From equation (2), the composite waveform will tell us if reflected waves have an impact or not on the amplitude of the first peak, which was the parameter analyzed by David, Sarout, et al. (2017).

## 3. Results

Table 1 summarizes our results for the critical distance, the angle of incidence, and the coefficient of reflection. The first and second columns of Table 1 indicate whether the observed amplitude of the first peak and $P$ wave velocity was either decreasing (D) or increasing (I) when the water rise first impacts the recorded waveforms. Qualitatively, our results show that there is a very good agreement between the amplitude variation (D or I) and the sign of the coefficient of reflection (negative or positive), except for two samples (CAT and EDB): This suggests that qualitatively, the interaction between direct and reflected waves can potentially induce the observed amplitude variation in agreement with the suggestion of Kovalyshen (2018).

### 3.1. Water Front Position Versus Critical Distance

Comparing the observed distance $d_A$ of the water front to the critical distance $z_c$, our results show that the condition $d_A < z_c$ is never fulfilled. Figure 1 shows that the offset between $d_A$ and $z_c$ is highly variable, with both small and large values. We expect (i) no impact in the samples with red symbols (measured distance higher than twice the critical distance), (ii) little impact in the samples with pink symbols, and (iii) significant impact for the samples with green symbols. However, the potential impact needs also to be quantified by taking into account the magnitude of the reflection coefficients.

### 3.2. Magnitude of the Coefficient of Reflection

Combining the results for planes 1 and 2 in Table 2, the distribution of $R_{\mathrm{PP}}$ values is shown in Figure 2. Most of the values are in the range $[-0.35; 0]$ with a strong peak in the range $[-0.1; 0]$ showing that the magnitude of the coefficient of reflection is generally very low. If the conditions are met for an interaction between direct

**Table 2**
*Critical Distance, Coefficient of Reflection, and Angle of Incidence on Planes 1 and 2*

| Sample | Observed amplitude variation (D) ecrease (I)ncrease | Observed velocity variation (D)ecrease (I) ncrease | Critical distance $z_c$ (mm) | Observed distance of water front $d_A$ plane 1 (mm) | Angle of incidence PLANE 1 (°) | Coefficient of reflection $R_{PP}$ plane 1 | Observed distance of water front $d_A$ plane 2 (mm) | Angle of incidence plane 2 (°) | Coefficient of reflection $R_{PP}$ plane 2 |
|---|---|---|---|---|---|---|---|---|---|
| SMX | D/D | D/D | 5.21 | 11 | 60.6 | −0.027 | 6 | 72.9 | −0.140 |
| CSG | D/D | D/D | 3.33 | 6 | 65.5 | −0.311 | 13 | 45.3 | −0.147 |
| MAJ | D/D | D/D | 4.56 | 9 | 65.2 | −0.127 | 17 | 48.9 | −0.037 |
| SH-ver | D/D | D/D | 4.21 | 16 | 50.6 | −0.113 | 26 | 36.9 | −0.063 |
| LEO | D/D | D/D | 4.15 | 10 | 52.6 | −0.054 | 17 | 37.6 | −0.021 |
| SH-hor | D/D | D/D | 3.71 | 5 | 75.6 | −0.328 | 15 | 52.4 | −0.069 |
| SID | I,D/I,D | I/I | 6.05 | 11 | 50.4 | 0.264 | 14 | 43.5 | 0.186 |
| BER | D/D | D,I/D,I | 3.96 | 7 | 62.9 | −0.159 | 13 | 46.5 | −0.071 |
| CAT | D/D | I/I | 3.92 | 5 | 70.3 | 0.990 | 7 | 63.4 | 0.990 |
| EDB | D/D | D,I/D,I | 5.01 | 8 | 59.6 | 0.004 | 13 | 46.4 | 0.021 |
| SAV | D,I/D | D,I/D,I | 4.65 | 6 | 65.7 | −0.048 | 6 | 65.7 | −0.048 |
| TUF | D/D | D/D | 3.61 | 6 | 65.8 | −0.287 | 8 | 59.1 | −0.208 |

*Notes*. The samples are those studied by David, Sarout, et al. (2017).

and reflected waves impacting the first peak of the waveform, our calculations show that the effect should small: In most of the cases the amplitude of the reflected *P* wave is about 10 to 20% that of the incident *P* wave. For one sample (CAT) we obtained a coefficient of reflection close to one: This case corresponds to total reflection as (i) the velocity in the wet rock is higher than in the dry rock and (ii) the angle of incidence is higher than the critical angle. For this sample a decrease of amplitude was observed when the water front was rising (Figure A1 in David, Sarout, et al., 2017), which by no means can be explained by the wave interaction mechanism suggested by Kovalyshen (2018) with a positive coefficient of reflection.

### 3.3. Composite Waveform Simulation

Using equation (2) it is possible to build a composite waveform and analyze the impact of the reflected wave on the first peal amplitude. This was done on three examples, each of them corresponding to a different colored symbol in Figure 1: (i) Sample SH-hor/ plane 1 (green symbol in Figure 1) has a small delay time ($t_R$ = 0.8 μs) and a large negative coefficient of reflection ($R_{PP}$ = −0.33), (ii) sample MAJ/plane 1 (pink symbol in Figure 1) has a higher delay time ($t_R$ = 1.8 μs) and a coefficient of reflection ($R_{PP}$ = −0.13) closer to the average value, and (iii) sample SH-ver/plane 1 (red symbol in Figure 1) has a much larger delay time ($t_R$ = 6.4 μs) and a coefficient of reflection with low magnitude ($R_{PP}$ = −0.11). As expected, the amplitude of the first peak is impacted only for SH-hor for which the observed distance $d_A$ was relatively close to the critical distance $z_c$

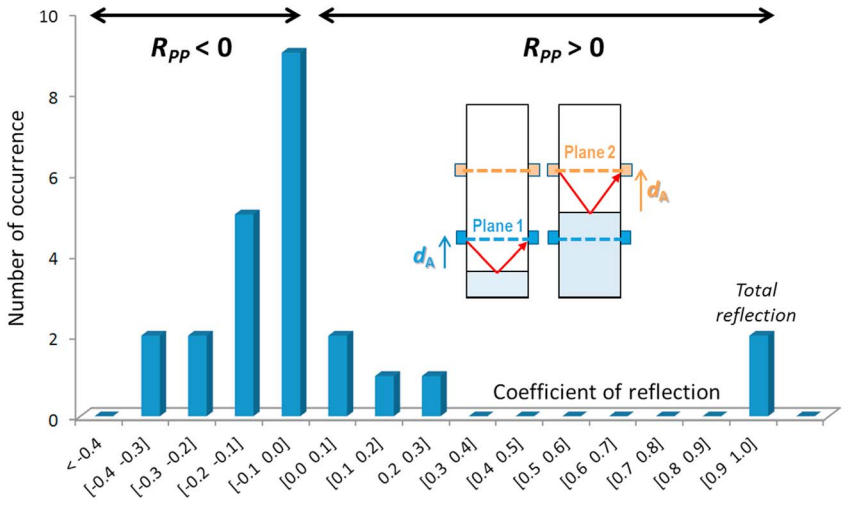


**Figure 2.** Histogram of the calculated coefficients of reflection $R_{PP}$ for both planes 1 and 2.

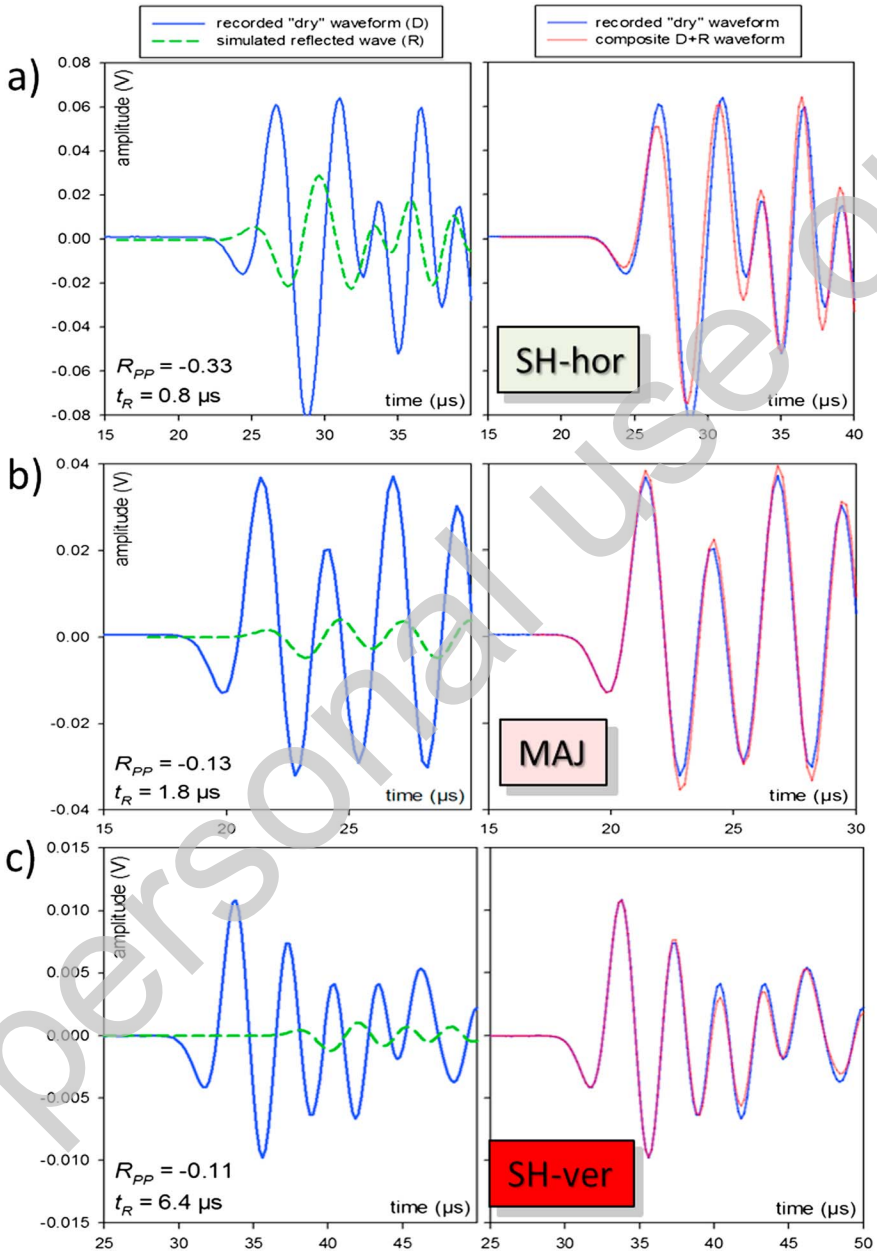


**Figure 3.** Construction of the composite waveform (red) from the recorded waveform of the dry sample (blue) and the simulated reflected wave (green). (a) Horizontal Sherwood sandstone (SH-hor) plane 1, (b) Majella grainstone (MAJ) plane 1, and (c) vertical Sherwood sandstone (SH-ver) plane 1.

(Figure 3a). For sample MAJ, the impact of the reflected wave is noticeable only on the second peak, while the first one is unchanged (Figure 3b). Finally, for sample SH-ver, the first amplitude variation occurs on the fourth peak only, and it is very small.

## 4. Discussion and Conclusion

The assumption that interacting *P* waves could be responsible for the observed amplitude variation before any velocity variation during capillary rise as suggested by Kovalyshen (2018) was checked on the complete data set presented in David, Sarout, et al. (2017). Our calculations show that the criterion proposed by Kovalyshen (2018) on the critical distance below which the first peak amplitude is impacted by the

reflected *P* wave is actually never fulfilled. In addition our data set allowed us to calculate for each sample the magnitude of the coefficients of reflection on the water front, and we found almost systematically very small values. Finally, we could check directly on the recorded waveforms if the alternative explanation holds: The analysis of the composite waveform on three examples shows that an impact on the first peak amplitude is expected at best in 5 situations out of 24 (the green symbols in Figure 1). Our conclusion, therefore, is that the *P* wave interaction is clearly a mechanism, which can lead to variations of the amplitude of the first peak and could impact the results for some of our rock samples (3 out of 12), but it is very likely that such a mechanism is not responsible for the early amplitude variation detected in the others (9 out of 12). Therefore, we still think that moisture diffusion is a very relevant mechanism to account for our observations presented in David, Sarout, et al. (2017).

In our calculations, we used the same assumptions as Kovalyshen (2018): The rising water front is assumed to be an horizontal plane, the ultrasonic emitters and receivers are considered as points, and plane waves are propagating. As a consequence, the conclusion suffers some weakness. In the future we plan to conduct additional numerical simulations which would take into account (i) the real geometry of the imbibition front and (ii) the characteristics of the seismic source (size of sensors, frequency content, directivity …), and by solving the full equations for wave propagation in heterogeneous media, we could get more realistic waveforms, to be compared to the recorded ones. Only such a comprehensive full wave modeling will allow us to provide satisfactory answers to validate or not the assumption of wave interaction suggested by Kovalyshen (2018).

**Acknowledgments**
We thank Yevhen Kovalyshen for suggesting another possible interpretation of our observations. The data presented in this work can be made available upon request.

## References

David, C., Barnes, C., Desrues, M., Pimienta, L., Sarout, J., & Dautriat, J. (2017). Ultrasonic monitoring of spontaneous imbibition experiments: Acoustic signature of fluid migration. *Journal of Geophysical Research: Solid Earth*, *122*, 4931–4947. https://doi.org/10.1002/2016JB013804

David, C., Louis, L., Menéndez, B., Pons, A., Fortin, J., Stanchits, S., & Mengus, J. M. (2013). X-ray imaging of fluid flow in capillary imbibition experiments. In K. A. Alshibli & A. H. Reed (Eds.), *Advances in computed tomography for geomaterials* (pp. 262–269). Hoboken, NJ: John Wiley.

David, C., Menéndez, B., & Mengus, J. M. (2011). X-ray imaging of water motion during capillary imbibition: Geometry and kinetics of water front in intact and damaged porous rocks. *Journal of Geophysical Research*, *116*, B03204. https://doi.org/10.1029/2010JB007972

David, C., Sarout, J., Dautriat, J., Pimienta, L., Michée, M., Desrues, M., & Barnes, C. (2017). Ultrasonic monitoring of spontaneous imbibition experiments: Precursory moisture diffusion effects ahead of water front. *Journal of Geophysical Research: Solid Earth*, *122*, 4948–4962. https://doi.org/10.1002/2017JB014193

Kovalyshen, Y. (2018). Comment on "Ultrasonic monitoring of spontaneous imbibition experiments: Precursory moisture diffusion effects ahead of water front" by C. David et al. *Journal of Geophysical Research: Solid Earth*, *123*. https://doi.org/10.1029/2018JB016040

Mavko, G., Mukerji, T., & Dvorkin, J. (2009). *The rock physics handbook—Tools for seismic analysis of porous media (2nd edition)*. Cambridge: Cambridge University Press.

Journal of Geophysical Research: Solid Earth

COMMENT
10.1029/2018JB016040

This article is a comment on David et al. (2017) https://doi.org/10.1002/2017JB014193.

**Key Point:**
- *P* wave reflection from imbibition front can explain amplitude change of recorded *P* waves

**Correspondence to:**
Y. Kovalyshen,
Yevhen.Kovalyshen@csiro.au

**Citation:**
Kovalyshen, Y. (2018). Comment on "Ultrasonic monitoring of spontaneous imbibition experiments: Precursory moisture diffusion effects ahead of water front" by David et al. (2017). *Journal of Geophysical Research: Solid Earth*, *123*. https://doi.org/10.1029/2018JB016040

Received 30 APR 2018
Accepted 17 JUL 2018
Accepted article online 27 JUL 2018

# Comment on "Ultrasonic Monitoring of Spontaneous Imbibition Experiments: Precursory Moisture Diffusion Effects Ahead of Water Front" by David et al. (2017)

**Yevhen Kovalyshen**[1]

[1]Energy, CSIRO, Perth, Western Australia, Australia

**Abstract** This brief note presents an alternative explanation to the fact that in the imbibition experiments with active ultrasonic monitoring the amplitude of the recorded *P* waves detects imbibition front before any changes in the *P* wave velocities are observable. The model is based on *P* wave interaction with the imbibition front. The qualitative estimation is in agreement with previously published experimental data.

**Plain Language Summary** In this note I comment on the recently published paper: David, C., J. Sarout, J. Dautriat, L. Pimienta, M. Michee, M. Desrues, and C. Barnes (2017), Ultrasonic monitoring of spontaneous imbibition experiments: Precursory moisture diffusion effects ahead of water front, J. Geophys. Res. Solid Earth, 122, 4948–4962. In particular, I provide an alternative, simpler explanation to the observed there phenomena that the amplitude of the recorded *P* waves detects imbibition front before any changes in the *P* wave velocities are observable.

## 1. Motivation

This report was motivated by the following recent papers on spontaneous water imbibition experiments: David, Barnes, et al. (2017) and David, Sarout, et al. (2017). In particular, these papers (see also David et al., 2015; Dautriat et al., 2016) present experiments in which moving water front was monitored using ultrasonic transducers (active acoustic monitoring). It was noticed that the amplitude of *P* waves dropped significantly before any changes in *P* wave velocity was detected. David, Sarout, et al. (2017) related this early change in amplitude to diffusion of moisture (water vapor) ahead of the water front. But why does the moisture diffusion affect only *P* wave amplitude but not the velocity? In the introduction David, Sarout, et al. (2017) cite a paper illustrating that relative humidity does affects both *P* wave amplitude and velocity. Therefore, it is questionable if indeed the diffusion of moisture (water vapor) ahead of the water front is able to explain why during imbibition process the *P* wave amplitude reacts ahead of the *P* wave velocity. In this report I present an alternative, much simpler explanation based on waves reflections and refractions.

## 2. Alternative Explanation

In this note I am presenting an qualitative analysis and I am not aiming to give any quantitative results. Let us assume that the water imbibes the porous medium in a piston-like manner, that is, the boundary between the water/vapor-invaded and air-saturated parts of the medium referred to as the imbibition front is sharp and flat (see Figure 1). Based on experimental data, I assume that the *P* wave velocity, $\alpha_{nw}$, in the air-saturated region is higher than the *P* wave velocity, $\alpha_{w}$, in the water-invaded region. Also, for illustration purposes, I assume point source and receiver. Let us now consider a case when the imbibition front is just below the transducers plane (see left of Figure 1). In this case the first break in the received signal corresponds to the *P* wave traveling along the shortest part connecting the transducers (the black line), while the signal reflected from the imbibition front (the blue line) arrives with a slight delay; see Figures 1 and 2. Note that the difference in the travel paths between the two signals is equal to

$$\Delta = \frac{L}{\sin i} - L = \sqrt{L^2 + 4z^2} - L \approx \frac{2z^2}{L}, \qquad \text{if} \qquad \frac{z}{L} \ll 1.$$

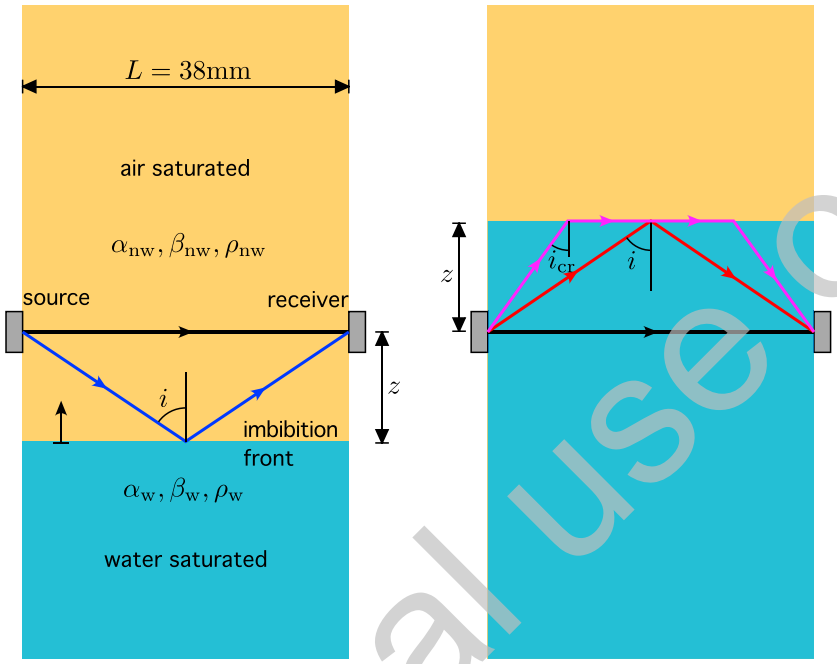


**Figure 1.** Sketch of imbibition and wave reflection paths.

If this difference is smaller than a quarter wavelength of the *P* wave signal, $\lambda$, then the first pick of the signal recorded by the receiver is affected by the reflection from the imbibition front; see Figure 2. In other words, if

$$\Delta \lesssim \lambda/4 \quad \Longrightarrow \quad z \lesssim 0.5\sqrt{\frac{\lambda L}{2}}, \tag{1}$$

then the direct and reflected waves interfere causing change in the amplitude of the recorded signal. Figure 3 illustrates the dependence of the reflection coefficient on the incidence angle; see Aki and Richards (1980). The values for the *P* velocities $\alpha_{\text{nw}}$ and $\alpha_{\text{w}}$ were taken from David et al. (2015), the case of the Saint-Maximin grainstone, while the *S* velocities $\beta_{\text{nw}}$ and $\beta_{\text{w}}$ were calculated assuming constant *Vs*/*Vp* ratio of 0.5. One can see that in the case of *P* wave coming from the dry region of the sample onto the imbibition front the reflection coefficient (blue line in Figure 3) is negative for the angle of incidence greater than 50°. This means that the phase of the reflected wave is shifted by 180° with respect to the direct wave; therefore, if inequality (1) is satisfied, the interference leads to decrease in the amplitude of the recorded signal; see Figure 2. In the case of $\alpha_{\text{nw}} = 2.74$ km/s and signal frequency of 0.5 MHz, the wavelength $\lambda \approx 5.5$ mm and inequality (1) leads to $z \lesssim 5.1$ mm and $i \gtrsim 74.4°$. It means that when the imbibition front is 5 mm away or closer, the amplitude of the recoded signal is lower compared to the amplitude of the undisturbed signal. Obviously, the reflection does

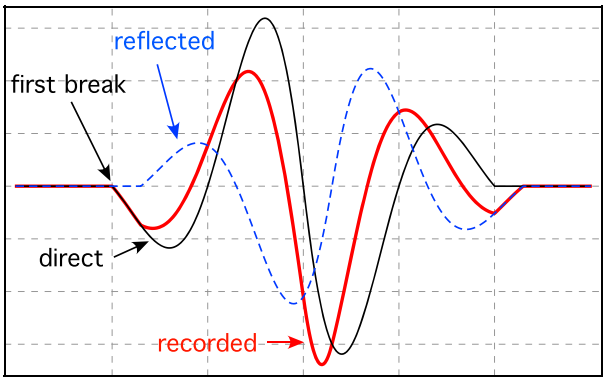


**Figure 2.** Illustration of wave interference.

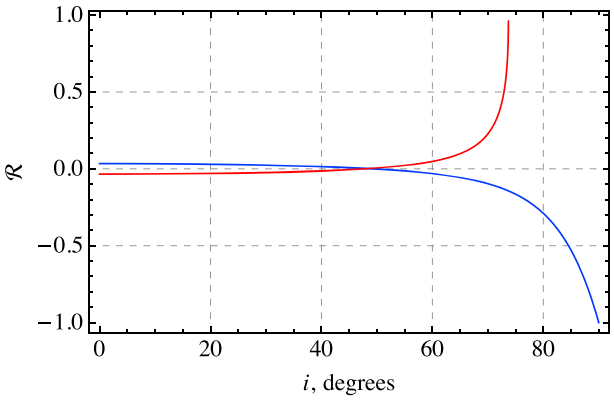


**Figure 3.** Reflection coefficient: $\alpha_{nw} = 2.74$ km/s, $\beta_{nw} = 0.5\alpha_{nw}$, $\rho_{nw} = 2.6$ g/cm$^3$, $\alpha_w = 2.63$ km/s, $\beta_w = 0.5\alpha_w$, and $\rho_w = 2.9$ g/cm$^3$, where $\beta_i$ is *S* wave velocity and $\rho_i$ is density. Blue/red lines correspond to incidence from air/water-saturated region and reflection back into air/water-saturated region.

not affect the first break of the recorded signal which still corresponds to the direct arrival; see Figure 2. Note that David et al. (2015) reported that in their experiment they started to detect the change in the amplitude when the visible imbibition front was 6 mm away from the transducers.

In the case when the imbibition front is above the transducers plane (see right of Figure 1) the first break would correspond to the arrival of the head wave (see magenta path). The measured *P* wave velocity changes linearly with respect to the position of the imbibition front $z$ starting from $\alpha_{nw}$ when the imbibition front is in the transducers plane and decreasing to $\alpha_w$ at some critical value of $z_{cr} = L/\left(2\tan i_{cr}\right)$, where $\sin i_{cr} = \alpha_w/\alpha_{nw}$ (see Figure 1). In the case of the above example $i_{cr} \approx 73.7°$ and $z_{cr} \approx 5.6$ mm. David et al. (2015) reported that the *P* wave velocity stabilizes by the time when the imbibition front is 10 mm above the transducers plane.

Here I presented only qualitative estimation, which are in agreement with published experimental data. Note that the present model hinges on a simplification of a flat discontinuous imbibition front. I do not claim that there is no moisture diffusion ahead of the visible water front. I just say that if there is any additional water-rock interaction ahead of the visible water front, for example, moisture diffusion, it should affect both the amplitude and velocity of *P* waves, while the fact that the *P* wave amplitude reacts ahead of the *P* wave velocity can be explained by *P* wave reflections and refractions. For quantitative computations one would require to run full numerical simulation that takes into account more realistic geometry of the transducers as well as of the imbibition front.

## References

Aki, K., & Richards, P. (1980). *Quantitative seismology: Theory and methods*. San Francisco: W.H. Freeman.

Dautriat, J., Sarout, J., David, C., Bertauld, D., & Macault, R. (2016). Remote monitoring of the mechanical instability induced by fluid substitution and water weakening in the laboratory. *Physics of the Earth and Planetary Interiors*, *261*, 69–87.

David, C., Barnes, C., Desrues, M., Pimienta, L., Sarout, J., & Dautriat, J. (2017). Ultrasonic monitoring of spontaneous imbibition experiments: Acoustic signature of fluid migration. *Journal of Geophysical Research: Solid Earth*, *122*, 4931–4947.

David, C., Bertauld, D., Dautriat, J., Sarout, J., Menéndez, B., & Nabawy, B. (2015). Detection of moving capillary front in porous rocks using X-ray and ultrasonic methods. *Frontiers in Physics*, *3*, 53.

David, C., Sarout, J., Dautriat, J., Pimienta, L., Michée, M., Desrues, M., & Barnes, C. (2017). Ultrasonic monitoring of spontaneous imbibition experiments: Precursory moisture diffusion effects ahead of water front. *Journal of Geophysical Research: Solid Earth*, *122*, 4948–4962. https://doi.org/10.1002/2017JB014193